Transpolar arcs: Seasonal dependence identified by an automated detection algorithm

G.E. Bower[1], S.E. Milan[1,2] and L.J. Paxton[3]

[1] University of Leicester, UK

[2] Birkeland Centre for Space Science, Bergen, Norway

[3] Johns Hopkins University Applied Physics Laboratory, USA

Key Points:

- An automated detection algorithm has been developed to identify transpolar arcs (TPAs) in DMSP-SSUSI data.
- There is a seasonal dependence in the occurrence of TPA such that they are detected more often in the winter hemisphere.
- There dawn/dusk DMSP/SSUSI orbit plane leads to UT biases in the polar cap sampling.

Abstract

Transpolar arcs (TPAs) are auroral features that occur polewards of the main auroral oval suggesting that the magnetosphere has acquired a complicated magnetic topology. They are primarily a northward interplanetary magnetic field (IMF) auroral phenomenon, and their formation and evolution have no single explanation that is unanimously agreed upon. An automated detection algorithm has been developed to detect the occurrence of TPAs in UV images captured from the Special Sensor Ultraviolet Spectrographic Imager (SSUSI) instrument onboard the Defense Meteorological Satellite Program (DMSP) spacecraft, in order to further study their occurrence. Via this detection algorithm TPAs are identified as a peak in the average radiance intensity poleward of 12.5° colatitude, in two or more of the wavelengths/bands sensed by SSUSI.

Orbital biases in the data have been investigated and these differ from spacecraft to spacecraft. For the spacecraft of interest (F16, F17 and F18) this leads to a preferential observation of the northern hemisphere with the detection algorithm missing TPAs in the southern hemisphere between approximately 01 - 06 UT. No seasonal bias has been found for these spacecraft.

Using the detection algorithm on observations from the years 2010 to 2016, over 5000 images containing TPAs are identified. The occurrence of these TPA images shows a seasonal dependence, with more arcs being visible in the winter hemisphere. We discuss the ramifications of these findings in terms of proposed TPA generation mechanisms.

Plain Language summary

Transpolar arcs (TPAs) are auroral features that occur polewards of the main auroral oval, at latitudes where auroras rarely form. TPAs occur primarily when the magnetic field embedded within the solar wind points northwards, the direction of Earth's magnetic field at the nose of the magnetosphere. Currently there is no single explanation for their formation and evolution.

An automated detection algorithm has been developed to detect the occurrence of TPAs in UV images captured from the Special Sensor Ultraviolet Spectrographic Imager (SSUSI) instrument onboard the Defense Meteorological Satellite Program (DMSP) spacecraft F16, F17 and F18. The three spacecraft together provide nearly continuous observation.

Using the detection algorithm on observations from the years 2010 to 2016, over 5000 images containing TPAs are identified. A clear dependence is seen such that more TPAs are identified in the winter hemisphere and no TPAs are identified between approximately 01 and 06 UT in the southern hemisphere. Orbital biases in the SSUSI data are able to explain the UT dependence but not the seasonal dependence thus suggesting there is a seasonal dependence on the detection

of TPAs.

1 Introduction

Transpolar arcs (TPAs) and polar cap arcs (PCAs) are auroral phenomena which lie poleward of the auroral oval and form during northward interplanetary magnetic field (IMF) when lobe reconnection can take place. TPAs/PCAs are usually Sun-aligned and can vary in type from theta aurora, which span the whole of the polar cap, to small scale arcs (Zhu et al., 1997; Zhang et al., 2016; Hosokawa et al., 2020). There is no clear distinction between TPAs and PCAs, the terms are used somewhat interchangeably. The existence of TPAs shows that the magnetosphere can have a magnetic topology that is distorted away from its textbook structure. This magnetic topology is poorly understood with many competing theories regarding the nature of the distortion and mechanisms for how this distortion arises. The aim of this paper is to investigate the seasonal occurrence of TPAs in 7 years of DMSP/SUSSI (Paxton et al., 1992, 1993, 2017) data from 2010 to 2016 to provide a greater understanding of the conditions that lead to TPA formation.

Currently there is no unanimously agreed upon formation model for TPAs. There are two main competing theories, the closed field line and open field line models. Milan et al. (2005) suggested that TPAs are produced by tail reconnection of open polar cap flux producing closed flux. This closed flux would usually return to the dayside as part of the Dungey cycle (Dungey, 1961), but Milan et al. (2005) argue that in a tail twisted by IMF B_Y-associated stresses, some of the flux becomes trapped and protrudes from the nightside into the polar cap. This model predicts the generation of asymmetric east-west ionospheric flows in the nightside auroral region (termed TRINNIs, tail reconnection during IMF-northward nonsubstorm intervals), and these have been observed at the same time as TPA formation (Milan et al., 2005; Fear and Milan, 2012b). The motion of the arc is then controlled by the rate of the lobe reconnection and the transport of open flux from one side of the arc to the other. Milan et al. (2005) noted that the arc's motion in the two hemispheres may not appear conjugate due to the differing lobe reconnection rates in either hemisphere, although the magnetic mapping between the hemispheres will be conjugate.

The open field line model suggests that TPAs should be associated with a convection shear or reversal boundary, requiring a field-aligned current and associated precipitation producing auroral emission. In this model, the precipitation producing the arcs should be embedded in a high-density polar rain. It has also been discovered that relativistic electrons and polar cap arcs

can occur on the same field lines in the central polar cap. This suggests that the magnetic field lines in the arc region are directly connected to the magnetosheath and the solar wind (Hardy et al., 1982; Zhu et al., 1997; Carlson and Cowley, 2005; Shi et al., 2013; Reidy et al., 2018) In this case there would be no reason for the TPAs to form conjugately in both hemispheres.

A key difference of these theories is whether TPAs form in both hemispheres or only in one. Another way to distinguish between the theories and the open or closed nature of the field lines is based on the presence of ion precipitation. Shinohara and Kokubun (1996) determined that electron precipitation accompanied by ion precipitation occurs on closed field lines. They showed that the precipitation does not significantly depend on the IMF B_X or B_Y. However if there is no accompanying ion precipitation the electron precipitation is believed to originate in the solar wind and as such is occurring on open field lines. Therefore if there is ion precipitation detected on the field line associated with the TPA, the TPA is believed to be consistent with the closed field line model. However if there is electron-only precipitation detected on the field line associated with the TPA, the TPA is believed to be consistent with the open field line model (Reidy et al., 2018).

Østgaard et al. (2003) reports two events in which a theta aurora is observed in one hemisphere and not in the other. They used IMAGE FUV SI13 in the northern hemisphere and Polar VIS Earth camera in the southern hemisphere and identified a TPA in the northern hemisphere on 5 November 2001 and in the southern hemisphere on 18 April 2001. Although the two cameras are operating at different wavelengths the auroral emission detected by both cameras is produced by electron impact on oxygen. Østgaard et al. (2003) also used DMSP-SSJ/4 particle data that showed ion precipitation consistent with closed field lines, but only in the hemisphere in which the TPA was seen. The lack of ion precipitation and visible TPA in the other hemisphere however is suggestive of open field lines. They suggest that the sign of B_X could explain why theta aurora can occur in one hemisphere. It can be seen that lobe reconnection is favoured in the northern hemisphere on the 5th November and the southern hemisphere on the 18th April due to the dipole tilt of the Earth and enhanced by a favourable B_X direction.

Conjugate polar cap arcs have been observed on few occasions due to the need for good observation of both hemispheres. Obara et al. (1988) used EXOS-C in the southern hemisphere, which identified intense electron precipitation on 25 September 1986, while Viking observed a TPA in the northern hemisphere. The precipitation had an energy spectrum similar to that of typical TPAs and the MLT sector of the precipitation matched that of the northern hemisphere arc. They suggested that the arc formed on closed field lines and was conjugate in both

hemispheres. Huang et al. (1989) showed a theta aurora in the northern hemisphere on March 25 1982 observed by Dynamics Explorer while ISEE 1 was located in the southern lobe of the magnetotail at 22.2 R_E. ISEE's particle observations suggested that there was also a TPA in the southern hemisphere, with the two being mirrored about the midnight meridian. Craven et al. (1991) used Dynamics explorer 1 in the southern hemisphere and Viking in the northern hemisphere to observe simultaneous TPAs in both hemispheres on 3 August 1986. They found that although the arcs were initially on different sides of the midnight meridian the motions of the arcs were independent. Carter et al. (2017) used IMAGE in the southern hemisphere and DMSP-F16-SSUSI in the northern hemisphere to track the motion of two coexisting arcs in both hemispheres on 31 August 2005. One of the arcs is almost static and stays close to the main auroral oval and the other moves across the polar cap. From the position of the arcs initially, they fit the Milan et al. (2005) model where the arcs are mirrored in each hemisphere about the midnight meridian. The motion of the moving arc is also as predicted by Milan et al. (2005) such that the arc moves towards the dusk in the northern hemisphere as $B_Y > 0$ and $|B_Y| > B_Z$. Xing et al. (2018) used ground-based Yellow River Station all-sky imager (Svalbard) to observed the northern hemisphere on 5 February 2006. Both hemispheres were also observed by space-based DMSP/SSUSI and NASA TIMED(Thermosphere Ionosphere Mesosphere Energetics and Dynamics)/GUVI (Global Ultraviolet Imager) instruments. TPAs appeared simultaneously in both hemispheres and lasted around 5 hours. The arc in the northern hemisphere formed on the duskside as an oval-aligned arc and in the southern hemisphere, it formed on the dawnside as would be predicted by the Milan et al. (2005) model.

Previous studies by Reidy et al. (2018) have used DMSP-SSUSI data along with DMSP SSJ/4 particle data to look at the interhemispheric nature of TPAs and determine if they occur on open or closed field lines. They identified 21 TPA events by eye for December 2015 that had corresponding particle data in at least one hemisphere. They found events consistent with both a closed field line model, arcs with ion signatures in both hemispheres, and the open field line model, arcs with electron-only precipitation as well as some events that were not consistent with either model.

Reidy et al. (2018) also studied TPA occurrence statistics and seasonal effects, looking at March, June, September and December 2015. They found that the percentage of TPAs recorded during the equinox months were similar, with approximately 40% in northern hemisphere and 60% in the southern hemisphere. For June and December the percentages were opposite, with the winter hemisphere seeing approximately twice as many TPAs as the summer hemisphere. They suggested that sunlight contamination prevents the identification of arcs in the summer

hemisphere and the DMSP orbits pass closer to the dayside in the northern hemisphere and closer to the nightside in the southern hemisphere, which is consistent with more arcs seen in the southern hemisphere during equinox months.

In this paper an automated technique is described to identify TPAs in UV images captured by the DMSP-SSUSI. DMSP does not allow the auroral dynamics to be examined due to relatively poor temporal cadence; however, we can investigate the interhemispheric nature of TPAs by using multiple spacecraft (F16, F17 and F18). This has allowed the seasonal occurrence of TPAs to be further determined, as well as the limitations of the SSUSI data due to orbital biases.

The instrumentation used in this study is described in section 2. Section 3 describes how the detection algorithm works. Section 4 shows the results of the detection algorithm when used between the years 2010 and 2016. It is broken down into 2 sections: in 4.1 the TPA images are considered independently, while in 4.2 multiple TPA images are collected together into TPA events. The results are discussed in Section 5. Section 5.1 focuses on the orbital biases in the DMSP/SSUSI data, specifically the seasonal bias (5.1.1) and the UT bias (5.1.2). Finally section 6 concludes.

2 Data

We employ auroral observations from the Special Sensor Ultraviolet Spectrographic Imager (SSUSI) instrument on board Defense Meteorological Satellite Program (DMSP) spacecraft F16, F17 and F18 (Paxton et al., 1992, 1993, 2017) https://ssusi.jhuapl.edu. The SSUSI instrument scans antisunward along its roughly dawn-dusk orbit and builds up an image of a swath of the polar regions over 20 minutes. SSUSI operates simultaneously at five wavelengths: 121.6 nm Lyman-α, 130.4 and 135.6 nm Oxygen lines and the Lyman-Birge-Hopfield bands, 140-150 nm short (LBHs) and 165-180 nm long (LBHl) (Paxton et al., 1992).

The DMSP spacecraft are at an altitude of 833 km (nominal) in 101.6 minute Sun-synchronous orbits, this therefore gives images for each hemisphere separated by approximately 50 minutes. All three spacecraft operate simultaneously during this time period, thereby providing near-simultaneous inter-hemispheric observations (Reidy et al., 2018). Figure 1a shows an example of the main auroral oval and a TPA, observed by DMSP-F16 on 25th December 2015. The TPA reaches across the polar cap from midnight to noon. The main oval is in general located at geomagnetic latitudes between 67 and 78° but some weaker emission extends to higher latitudes.

We also employ interplanetary magnetic field (IMF) data from the OMNI dataset with 1 minute cadence (King and Papitashvili, 2005).

3 Detection Algorithm

The detection algorithm uses the DMSP/SSUSI data from 130.4 and 135.6 nm Oxygen lines and the Lyman-Birge-Hopfield bands 140-150 nm short (LBHs) and 165-180 nm long (LBHl) only, this is because the Lyman-α data is not very clear in comparison to the other wavelengths. This most often arises because the ubiquitous geocoronal H Lyman-α emission is often far brighter than the auroral signal. Figure 1b is a visual representation of the detection algorithm in all four wavelengths. The detection algorithm works by first identifying the area above 12.5° colatitude, which we refer to as the detection window. 12.5° is used in order to maximise the area of the image checked whilst minimising the amount of times the auroral oval is inside the detection window. The radiance intensity inside the detection window is then averaged vertically (noon-midnight), shown by the faint grey line in Fig. 1b. The averaged radiance intensity is then smoothed using a boxcar method (black line in Fig. 1b). The maximum and minimum of the smoothed average radiance intensity is recorded for each wavelength.

For each wavelength the maximum and minimum of the smoothed average radiance intensity are tested against the upper and lower quartiles respectively of the maximum average radiance intensity of 2015. If the minimum of the average radiance intensity of the tested image is less than the lower quartile of 2015 and the maximum is greater than the upper quartile a potential TPA is identified. The reasoning for this is that usually there is no aurora in the polar cap above the 12.5° colatitude therefore by the maximum being greater than the upper quartile and the minimum being less than the lower it is more likely to be a real arc and not an image with high intensity over the whole plot.

If a potential TPA is identified in at least two wavelengths the image is recorded to be checked by eye. The potential TPA was chosen to be seen in at least two wavelengths to reduce the number of false positives, as discussed in more detail below. This criteria does however also reduce the number of real TPAs identified by the detection algorithm but when trialing one-wavelength and two-wavelength criteria it was found that the latter was more robust.

An important thing to note is the visual similarities between TPAs and bending arcs. Bending arcs are not TPAs and are the ionospheric flow and auroral response to a pulse of dayside reconnection liked to flux transfer events (FTEs). FTEs manifest as poleward-moving auroral forms which break away from the dayside auroral oval and progress a short distance into the

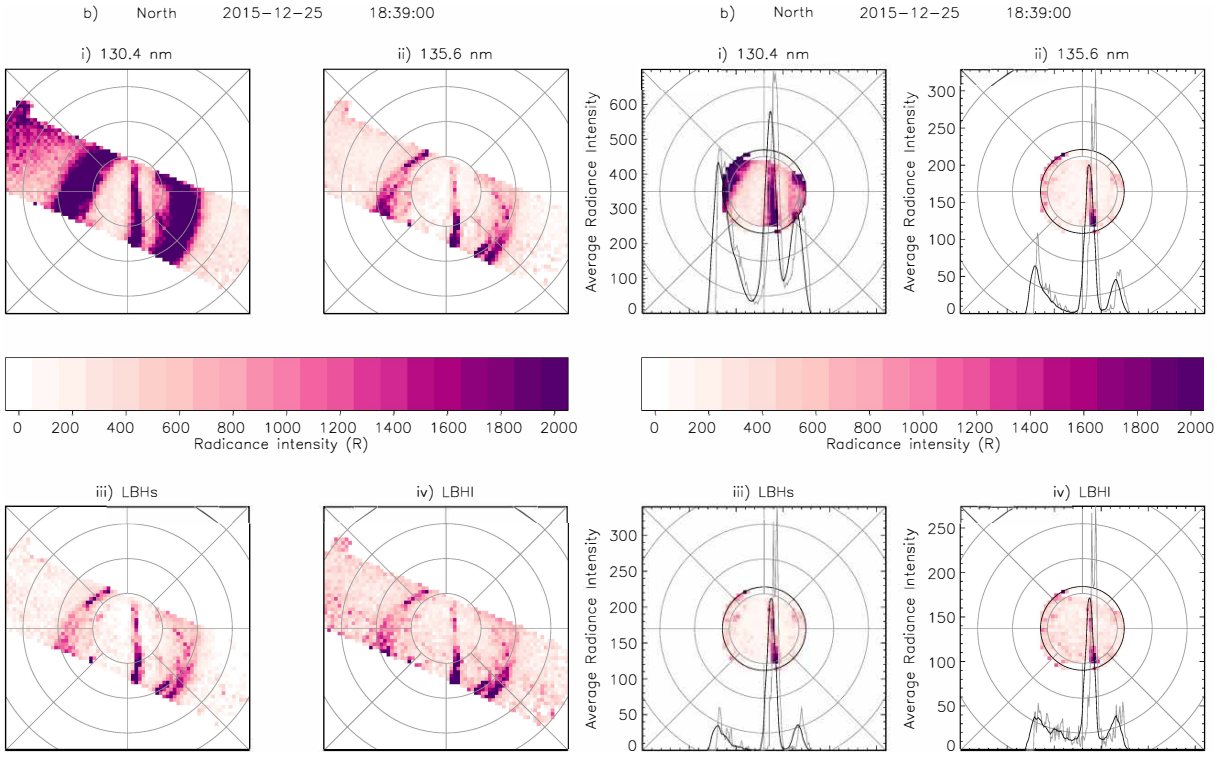

Figure 1: Data are presented in a magnetic latitude and magnetic local time frame, with noon at the top and dawn at the right circles show magnetic latitudes in steps of 10 degrees. (a) DMSP/SSUSI-F16 data showing a TPA on 25th December 2015 in northern hemisphere in wavelength i) LBHl ii) LBHs iii) 135.6 nm vi) 130.4 nm and (b) Breakdown of detection algorithm on this data. Inside black circle is DMSP-SUSSI data above 12.5° colatitude. Over-plotted is the average radiance intensity, grey line and the smoothed average radiance intensity, black line.

polar cap before fading. Bending arcs form under dominant IMF B_Y which results in a strong asymmetrical distribution of newly added flux to the polar cap. The arc then forms due to precipitation along the leading edge of newly opened field lines. As the newly open flux is re-distributed in the polar cap by the ambient convection field, the bending arc moves away from the oval (Carter et al., 2015; Kullen et al., 2002, 2015). The potential TPA images have to be checked by eye to remove bending arcs.

Checking by eye also removes other false positives, examples of which are shown in Figure 2. Fig. 2 shows three examples (a,b,c) with images in the four wavelengths for each example. Fig. 2a is when SSUSI has a high intensity over the majority of the image, probably due to sunlight contamination, this example being from northern hemisphere summer solstice conditions. Also F17 has a very poor response at 1304 and 1356 due to an issue the the grating which leads to some false positives. The criteria in the detection algorithm forcing the minimum of the average radiance intensity reduces the number of these false positive but some inevitably slip though due to the limited coverage that SSUSI provides. Fig. 2b is when the main auroral oval enters

the detection window and is misinterpreted as a TPA. This occurs most often when the dawn oval is at very high latitudes. The third example Fig. 2c is when the whole detection window is not scanned and a part is left untested, therefore insufficient area of the polar cap is sampled to give a reliable measure of the average radiance intensity.

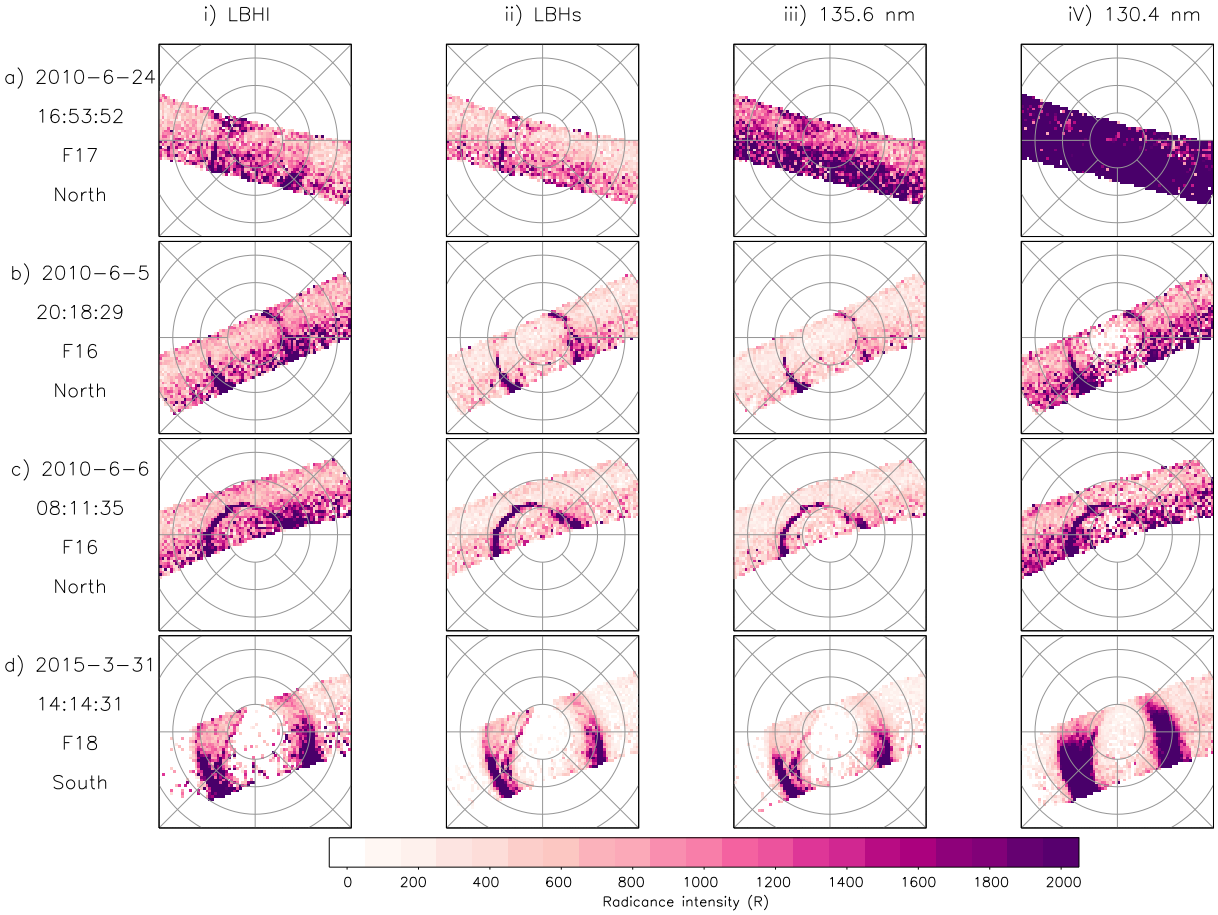

Figure 2: False positive detections. Data are presented in a magnetic latitude and magnetic local time frame, with noon at the top and dawn at the right; circles show magnetic latitudes in steps of 10 degrees. (a) High intensity over the whole image. (b) Auroral oval enters detection window. (c) Detection window not fully imaged. (d) Bending arc.

4 Observations

4.1 TPA Images

Running the detection algorithm for the years 2010 to 2016 identifies 11548 TPA images from the 211705 DMSP/SSUSI images. Of the 11548 potential TPA images 5698 are real TPA images and 360 are bending arc images (an example of which is shown in Fig. 2d), the remainder are false positives. Therefore, the detection rate has a success rate of $\sim 53\%$.

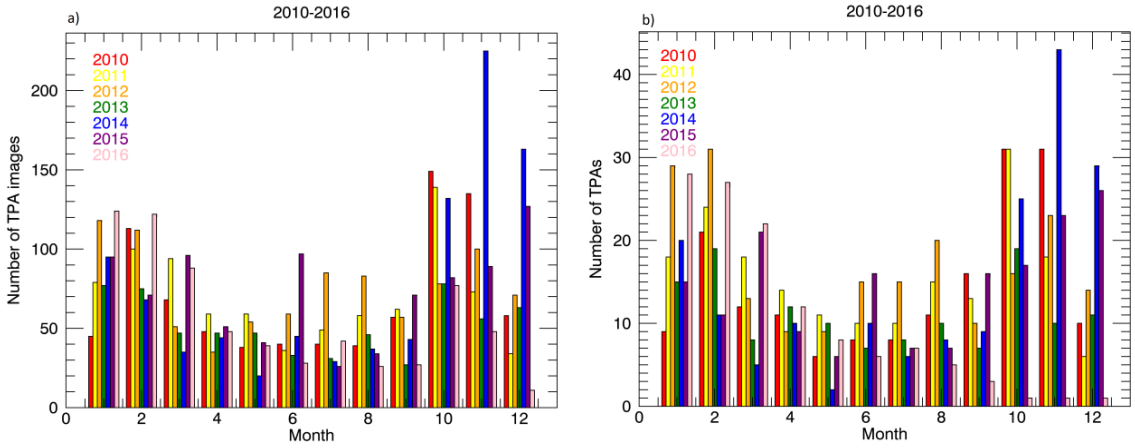

Figure 3: (a) Number of TPA images per year by month for 2010-2016. (b) Number of TPA events per year by month for 2010-2016.

Figure 3a shows the number of TPA images identified by month for each year. Across all seven years fewer TPA images are identified between approximately April and September. This could be due in part to the higher solar illumination in the northern hemisphere. The distribution across years appears roughly uniform, as shown in Figure 4, with no clear link to, say, the solar cycle. There are a few months, particularly October, November and December 2014, where more TPA images are identified.

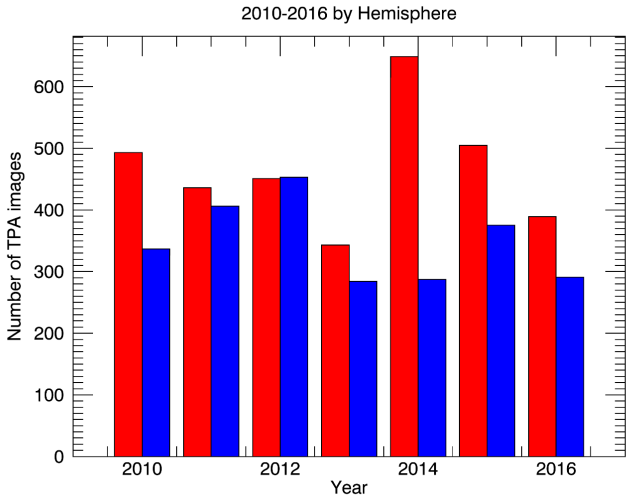

Figure 4: Number of TPA images per year by hemisphere for 2010-2016. The Northern Hemisphere is red and the Southern Hemisphere is blue.

	2015	March	June	September	December
(Reidy et al., 2018)	No. TPA images	333	228	327	204
	No. TPA events	50	42	41	43
	North (%)	41.3	30.7	39.4	67.2
	South (%)	58.3	69.3	60.6	32.8
Our findings	No. TPA images	108	102	92	138
	No. TPA events	58	39	42	76
	North (%)	37.0	23.5	37.0	94.9
	South (%)	63.0	76.5	63.0	5.1

Table 1: Number of TPA images and events for March, June, September and December 2015.

Reidy et al. (2018) has previously identified TPAs in DMSP/SSUSI data from spacecraft F16, F17 and F18 for March, June, September and December 2015. Comparing with their study, we find that fewer TPA images are identified by the detection algorithm (Table 1). Events are defined in section 4.2. The difference between the number of TPAs identified by Reidy et al. (2018) and this detection algorithm can be explained by the restrictions of the automated detection algorithm and it missing certain TPAs. This may be because the TPA may not have entered the detection window above 12.5° colatitude or that it may not be visible in two or more of the wavelength/bands or the maximum and minimum criteria of the average radiance intensity may not be met. Although less TPAs are detected it is a representative sample of the overall distribution. The percent in each hemisphere are similar between the two studies, with the equinoxes having comparable percentages and more TPA images in the winter hemisphere for the solstices.

The IMF clock angle is calculated at the time of each of the TPA images. Figure 5 shows the occurrence distribution within eight 45° sectors centered on 0°. As expected, the majority occur during northward IMF. The few percent that occur during southward IMF is most likely due to variability of the IMF such that it could have changed between the TPA forming and being imaged.

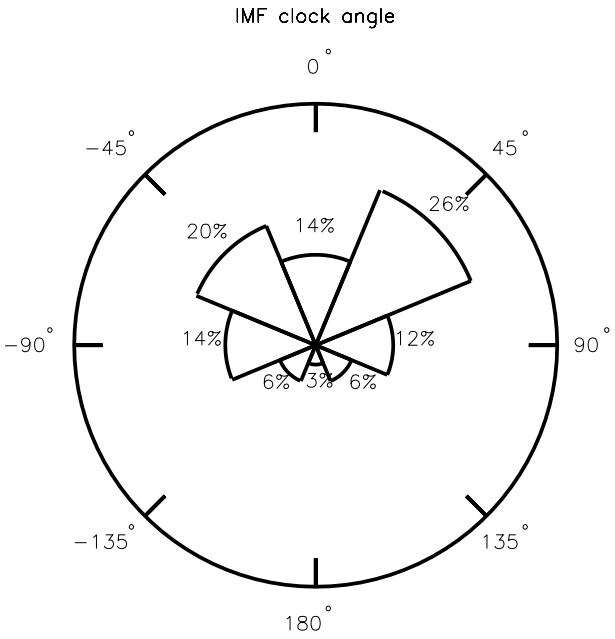

Figure 5: The percentage of TPA images with IMF clock angle split into 8, 45° sectors. The outer circle highlights the centre angle in degrees for each sector.

In figure 6 we combine the data from all the years to investigate the number of TPA images identified by each spacecraft in each hemisphere by month (Figure 6a-c) and by UT (Figure 6d-f). From Fig. 6a-c a clear seasonal dependence can be seen such that there are more TPA images identified in the winter hemisphere. There is also a UT dependence in Fig. 6d-f where no TPA images are identified in the southern hemisphere between $\sim$ 01-06 UT, with a strong peak at 16-17 UT. These dependences are investigated further in section 5.1.

Approximately the same distribution is seen for all three spacecraft. F17 has less northern hemisphere images between April and August and the UT panel peaks higher at 10 UT in the northern hemisphere. F18 has more southern hemisphere images with the peaks in the winter hemisphere being comparable to each other.

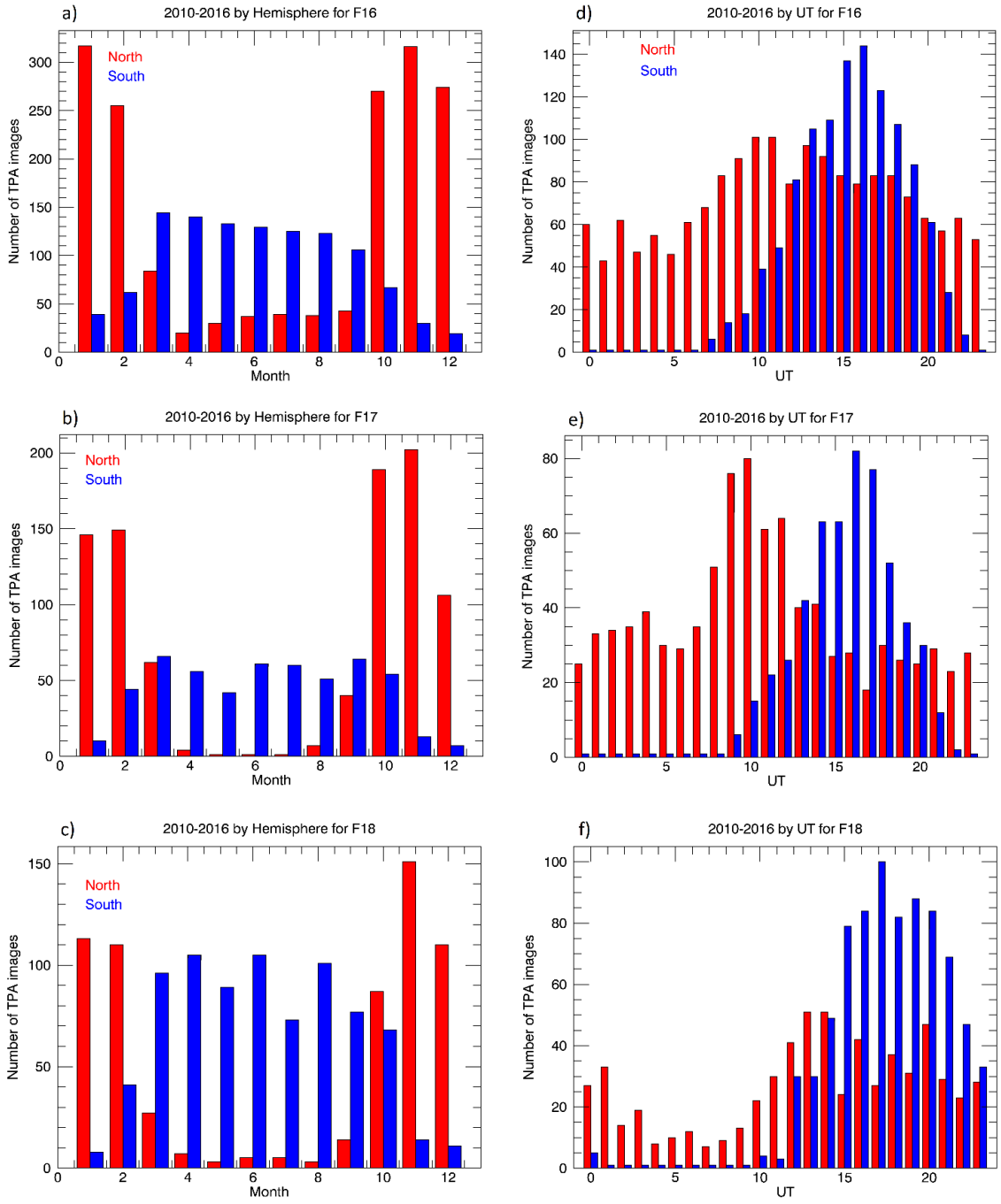

Figure 6: Number of TPA images for each Spacecraft combining all TPA images from 2010-2016. Top to bottom) spacecraft F16, F17 and F18. northern hemisphere is red and Southern blue. (a-c) Number of TPA images per hemisphere by month for each Spacecraft. (d-f) Number of TPA images per hemisphere by month for each Spacecraft.

4.2 TPA events

In order to see the hemispherical nature of the TPA, whether they occur in one hemisphere or both hemispheres, the TPA images have been combined into TPA events based on the time between the images. If the time between images containing TPAs is less than 90 minutes then the images are considered to be of the same event. The hemispherical nature of the TPA events is then determined from the hemispheres of TPA images that make up that event. If all the images are from one hemisphere the event is classified as a one-hemisphere event. If one or more images are from opposite hemispheres the event is classified as a two-hemisphere event. 90 minutes is chosen based on the orbit of the spacecraft such that a TPA has to be identified either in both hemispheres by at least one spacecraft or in one hemisphere by more that one of the spacecraft. If the image does not have another within 90 minutes the image is left unclassified. 1172 TPA events are identified. Figure 3b is in the same format as Fig. 3a but for the TPA events. The same pattern is seen for the TPA images (Fig. 3a) and the TPA events (Fig. 3b) with less TPAs occurring between approximately April and September. This shows that TPA events are not of a longer duration between October and March but there are more TPA events.

The number of events are comparable to those found by Reidy et al. (2018) except for December where more events are found using this method. This can be explained by the difference between the way images are turned into events here and by Reidy et al. (2018). Reidy et al. (2018) does not use a time constraint, as used here, but compares every image. To be classified as a two-hemisphere event by Reidy et al. (2018) the TPA must be visible in two subsequent images, one in each hemisphere. One-hemisphere events are classified by Reidy et al. (2018) if the TPA is absent from one hemisphere for all the spacecraft (F16, F17 and F18) and still present in the subsequent images of the original hemisphere.

The main difference between the two definitions of events is that one uses a time constraint and the other is based on the subjective decision as the whether the TPA is visible in subsequent images or not. The definition used here is more robust and based less on interpretation. However along with the limitations of the detection algorithm, the time constraint we employ is a harsher criterion to be met as can be seen from Table 2, which shows the difference in classification of the December 2015 TPAs, as more events are left unclassified. As such, it is possible that some of these unclassified TPAs are of the same event.

The TPA events are separated by hemisphere in Figure 7a-d. The left panel is events that are classified as one-hemisphere, in that it is observed in a single hemisphere by multiple spacecraft and not in the opposite hemisphere. This hasn't taken into account if the viewing is poor in

December 2015	(Reidy et al., 2018)	Our findings
Both hemispheres	19	5
One hemisphere	8	21
Unclassified	16	50

Table 2: December 2015 classifications of TPA events.

the other hemisphere. The same variation is seen here as in Fig. 6a-c such that there are more TPA events identified in the winter hemisphere. The right panels of Fig. 7 show events that have been classified as two-hemisphere events, such that a TPA image has been identified in both hemispheres by either one spacecraft or multiple spacecraft. In this panel more TPAs are identified in February and October.

The TPA events are separated by hemisphere and UT in Figure 7c-d. The left plot shows events that are classified as one hemisphere. The same variation is seen here as in Fig. 6d-f such that there are less TPA events in the southern hemisphere between 22-09 UT and a peak around 17 UT. The right panel of Fig. 7 shows events that have been classified as two-hemisphere events. This follows a similar pattern to the southern hemisphere of the one-hemisphere events.

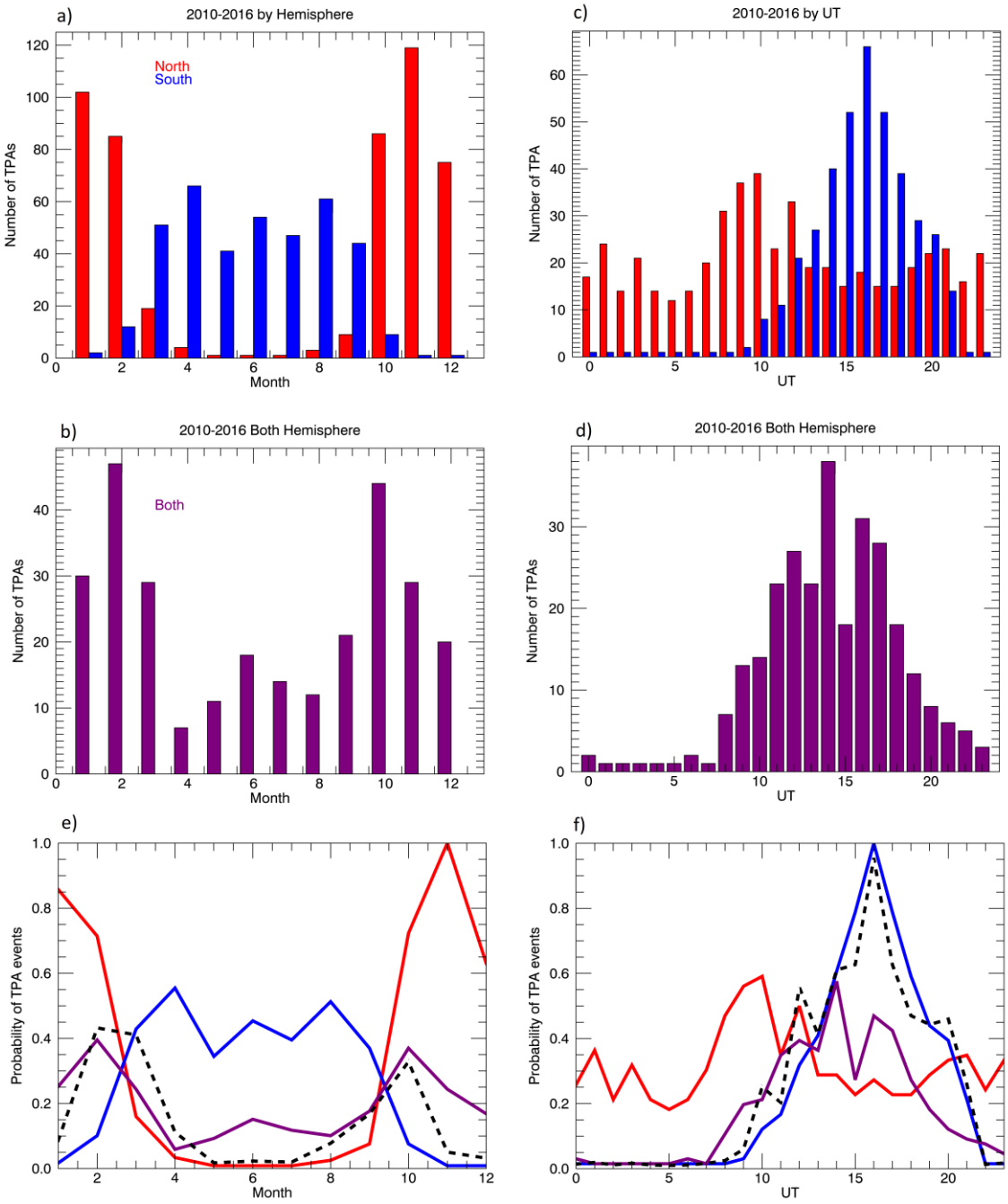

Figure 7: Number of TPA events per hemisphere combining all TPA images from 2010-2016 by (a-b) Month and (c-d) UT. Left) One hemisphere events, northern hemisphere is red and Southern blue. Right) Both hemisphere events, in purple. (e-f) Probability distributions. The black dashed line is the probability of a TPA being detected in both hemispheres.

4.3 Location of TPA

From the detection algorithm the location of the peak in average radiance intensity is recorded. This can be used a proxy of the location of the TPA across the dusk-dawn meridian, as it is the location of the brightest section of the TPA. This has an uncertainty of ±4.8° colatitude on the location of the TPA. There are also a few cases where the auroral oval is the brightest section and as such, the location of the TPA is falsely recorded on the opposite side of the midnight meridian, this occurs approximately 10 % of the time. Splitting the polar cap into dusk and dawn the number of TPA images detected in each sector is shown in Figure 8a split by hemisphere. The error bars in Fig. 8a include the ±4.8° colatitude uncertainty and the 10% error for TPAs classified on the wrong side of the midnight meridian.

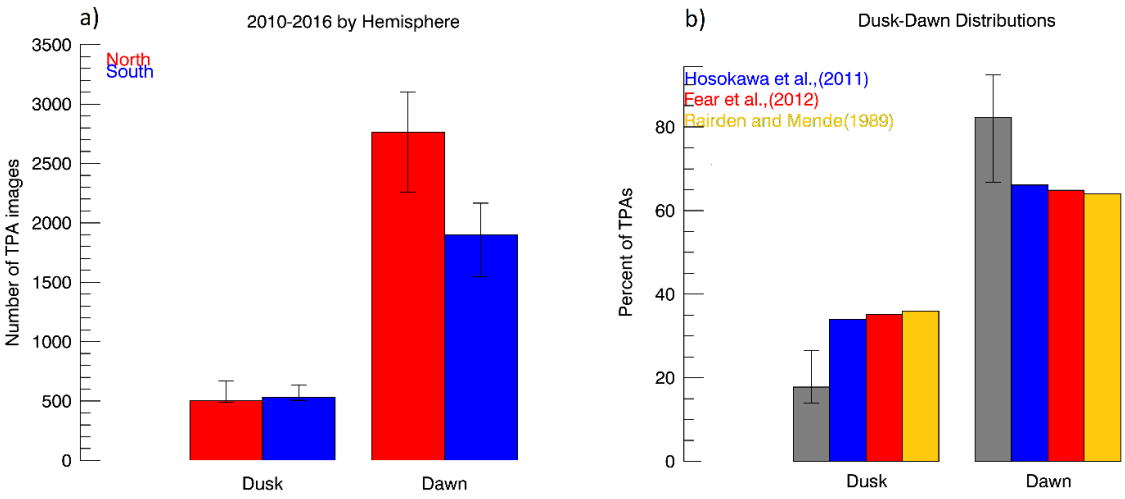

Figure 8: Dusk-dawn distributions. (a) Number of TPA images by location and hemisphere. (b) Number of TPA images at dusk and dawn for several studies. (Fear and Milan, 2012a; Hosokawa et al., 2011; Rairden and Mende, 1989).

From this, it can be seen, even with the error bars, that there is a clear dusk-dawn asymmetry such that TPAs are detected more often in the dawn sector. This distribution is investigated further with Fig. 8b in section 5.2.

5 Discussion

5.1 Orbital Biases

5.1.1 Seasonal Bias

The distributions show seasonal and UT dependences; here we investigate if these could be explained by the orbit of the spacecraft. The proportion of the detection window which gets scanned is dependent on the track of the spacecraft across the polar regions. The area scanned by DMSP/SSUSI for the months of June and December 2015 in the northern and southern hemispheres are shown in Figure 9a-c (The darker the colour the more times taht an area has been scanned by SSUSI). From these it can be seen that there is little variation between each month in the overall coverage of the polar cap, so cannot explain the seasonal dependence seen in Fig. 6a-c

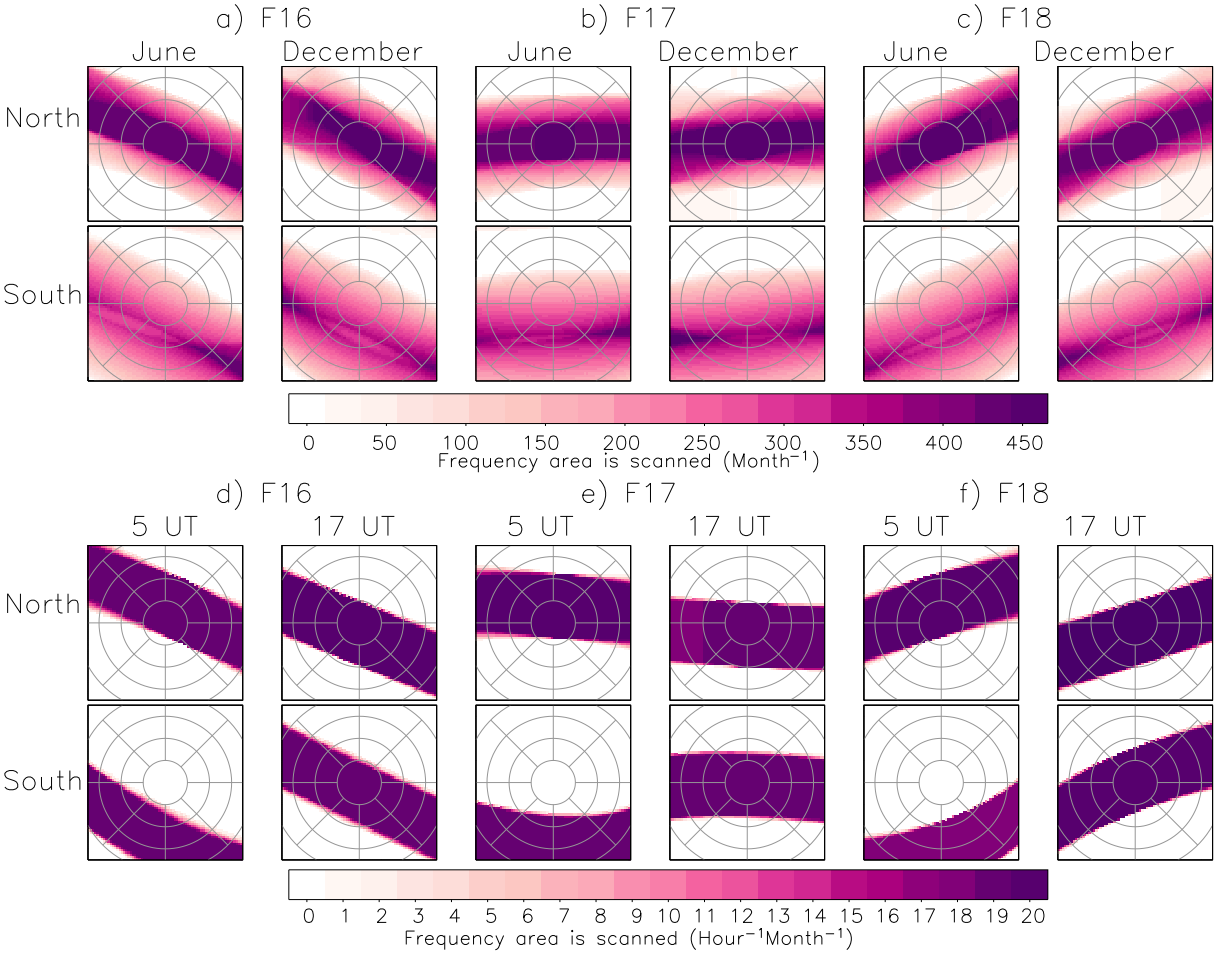

Figure 9: Frequency of the area scanned by SSUSI for Northern and Southern Hemisphere. (a-c) for June and December 2015. (d-f) at 5 and 17 UT for January 2015.

It can be seen that the spread of the area imaged by SSUSI is wider in the southern hemi-

Hemisphere	F16	F17	F18	Total
North	1938	1034	785	3755
South	1242	606	913	2761

Table 3: Number of TPA images per hemisphere for each spacecraft.

sphere thus leading to more times when the detection window is not fully imaged, accounting for the hemispherical bias in the number of TPAs seen (2761 Southern to 3755 Northern images). F18's result in Fig. 6a-c is different as it detected more arcs in the southern hemisphere than the Northern (table 3). This supports the possibility that the difference in occurrence of TPAs in the winter hemisphere is due to less data in the southern hemisphere.

The seasonal dependence of one-hemisphere TPAs (Figure 7b) is in agreement with the one hemisphere TPAs of Østgaard et al. (2003), where their TPAs form in the winter hemisphere (northern hemisphere for the November 5 2001 arc and southern hemisphere for the April 18 2001 arc).

5.1.2 UT Bias

We examined the UT and seasonal sampling distribution to determine that the seasonal dependence in the observations of TPAs is not an artefact of the spacecraft orbits. The area scanned by SSUSI for each spacecraft are plotted for January 2015 at 5 and 17 UT in Figure 9d-f, in which the geomagnetic pole in the northern hemisphere is tilted towards the Sun at 17 UT and away from the Sun at 05 UT. There is a clear variation in the spacecraft track across the polar regions for all three spacecraft, especially in the southern hemisphere, leading to a UT dependence in the coverage of the high-latitude regions by DMSP/SSUSI. The majority of the SSUSI scan is anti-sunward of the spacecraft track, so especially at 05 UT in the southern hemisphere the detection window is poorly sampled and few TPAs will be detected by the algorithm. This is consistent with the UT dependence seen in Fig. 6d-f.

As shown in Figure 9d-f, as the spacecraft image the area anti-sunward of their track, all the spacecraft provide good imaging of the detection window at all UT in the northern hemisphere. Comparison with Fig. 6d-f shows as expected that the number of TPA images is greatest for F16 when the spacecraft track is most favourable, passing close to the sunward edge of the detection window. The dip in the number of TPA images for F18 coincides with the times the spacecraft is furthest away from the detection window possibly missing some TPAs which form closer to midnight. In the same way, the dip and peak in F17 northern hemisphere data can be

explained, with fewer TPA images between 03-06 UT as the spacecraft track is at it furthest from the detection window and a peak at 09-11 UT where the spacecraft track is most favourable. However there are fewer images at 12 UT than would be expected.

The southern hemisphere high-latitude regions are not imaged at all UT. All three spacecraft do not image the detection window well between 23 and 08 UT with this extended to 10 and 11 UT for spacecraft F17 and F18 respectively. This is shown clearly in Fig. 6d-f with the number of TPA images being greatest for the southern data when the spacecraft track is most favourable and none when the detection window is not imaged. The angle with respect to the dawn-dusk meridian also affects the area imaged, being of most effect for F16 and F18 and results in the left (right) hand side of the detection window being missed for F18 (F16).

The orbital biases are quantified in Figure 10, which shows the average percent of the detection window scanned by the SSUSI instrument split for each spacecraft by hemisphere and month in Fig. 10a-c and by UT in Fig. 10d-f. From this the UT dependence is clear with the best coverage of the detection window in both hemispheres being between 11 and 20 UT for each spacecraft. The northern hemisphere coverage for F18 is also less than the other spacecraft which results in a more comparable number of northern and southern hemisphere arcs being detected (Table 3). The seasonal dependences seen for each spacecraft in Fig. 9a-c are not similar to the seasonal variation in the TPAs nor to each other. F16 (Fig.9a) has reduced coverage in both hemispheres for August-December. F17 (Fig. 9b) has reduced coverage in both hemispheres in April-July as well as December. F18 (Fig. 9c) has more variation in the northern hemisphere than the southern. The difference between the height of the northern and southern hemispheres averages can be explained by the UT dependence as there are less UT that provide good coverage in the southern hemisphere. Combining these differences does not explain the variation in season in the number of TPAs, hence we conclude that the seasonal dependence in the observations of TPAs is not an artefact of the spacecraft orbits.

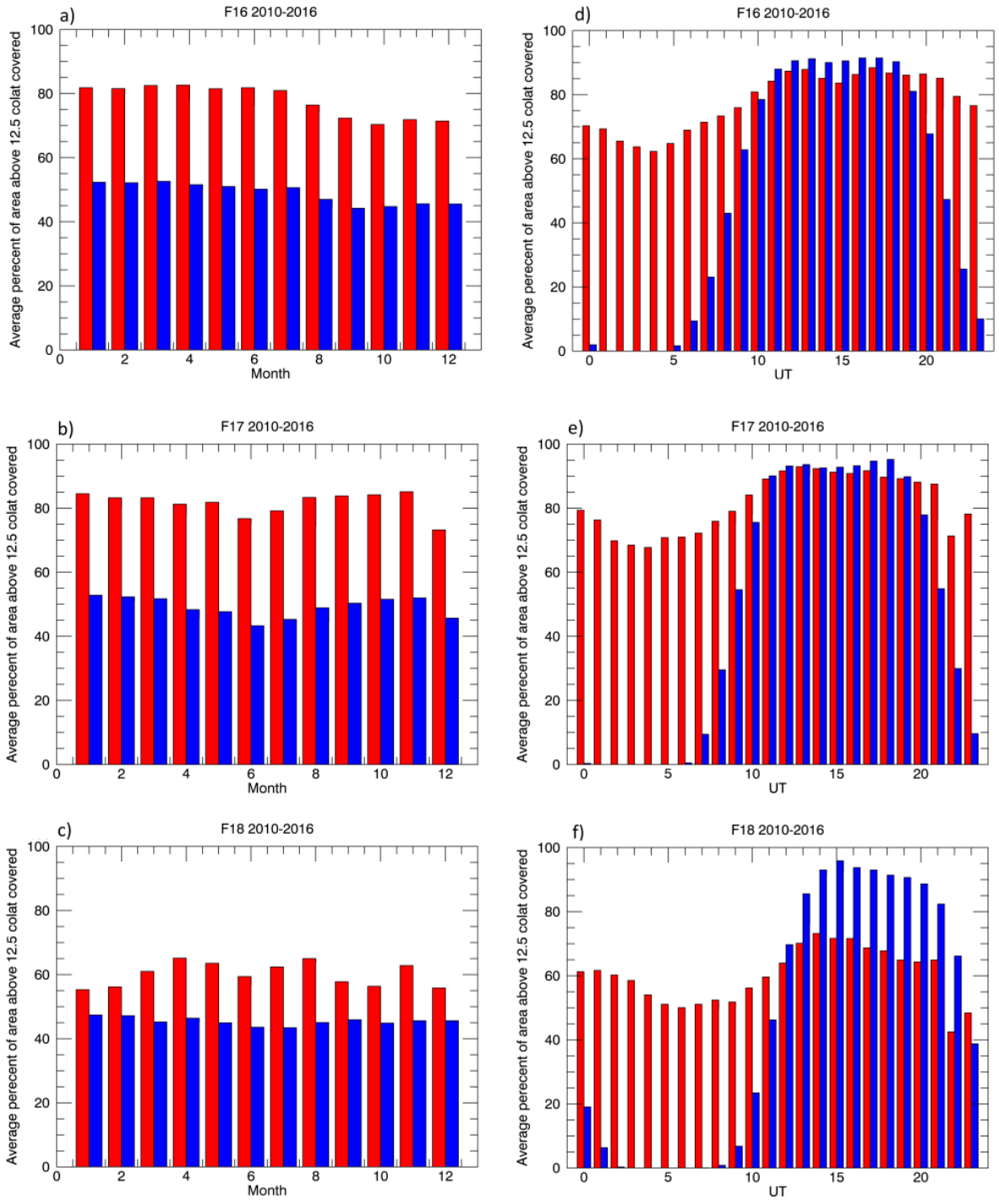

Figure 10: Average percent of the detection window scanned. (a-c) by month (d-f) by UT Top to bottom) Spacecraft F16, F17 and F18. Red is northern hemisphere Blue is southern hemisphere.

In order for the detection algorithm to work optimally full coverage of the detection window would be required, however this is rarely the case, occurring only 7% of the time. The detection algorithm is able to work with partial coverage, though it leads to some TPA images being

missed. Reidy et al. (2018) suggested that that TPAs are present in 20% of DMSP/SSUSI images from 2015. Assuming this can be extrapolated to other years this suggests that there could be up to 42,000 TPA images between 2010 and 2016 (there are 211,705 SSUSI images). However, the restriction in the detection algorithm means fewer are detected. The detection window is only sufficiently covered to identify TPAs a fraction of the time as shown in table 4. The expected percentage of TPA images identifiable is reduced based on the amount of the detection window scanned. This suggests that up to 28,500 TPA images are identifiable based on the spacecraft coverage of the detection window.

Percent of image scanned	Number of SUSSI images	Expected percentage of TPA images identifiable	Number of TPA images
≥ 75	120,539	20	24,107
$50 \leq x < 75$	17,415	10	3,483
< 50	55,940	5	890
		Total	28,480

Table 4: Number of TPA images expected to be detected by the detection algorithm

There are other restrictions in the detection algorithm which will lead to some TPA images being missed. The restriction of the TPA being identified in more than one wavelength leads to approximately 20 TPA images missed each month (1680 TPA images over the whole 7 years). Then there is the average radiance intensity restriction which requires the TPA's average radiance intensity to be sufficiently high. Assuming approximately 25% do not meet this condition 7120 images are missed. 25% is chosen as the detection algorithm requires the average radiance intensity to be above the upper quartile of 2015, and there are 25% that are above the mean but are not included as this would lead to too many false positives.

Combining these arguments, this suggests that the detection algorithm should be able to detect 19,680 TPA images. As only 11,548 TPA images are identified this leaves 8,132 (29%) images missed most likely due to non-standard auroral configurations.

5.2 Discussion

The detection algorithm successfully detects 5,698 TPA images in the DMSP/SSUSI data by identifying peaks in the average radiance intensity above 12.5° colatitude in two or more wavelengths (Fig. 1b). There is a seasonal dependence (Fig. 6a-c) such that more TPA images

are identified in the winter hemisphere, and a UT dependence (Fig. 6d-f) such that less TPAs are seen between $\sim$ 00 and $\sim$ 10 UT. The orbital biases of the DMSP spacecraft (Fig. 9a-c and Fig. 9d-f) can fully explain the UT dependence of the TPAs but are unable to explain the seasonal dependence. This is because the track that the spacecraft takes across the polar regions changes with UT but not as significantly with the month. When the spacecraft passes closer to the nightside this causes potential TPAs to be missed by the detection algorithm as the detection window is only partially scanned. This happens more frequently for the southern hemisphere than the northern hemisphere and occurs at different UT for each spacecraft. With all three spacecraft the detection algorithm is unable to detect TPAs between 01 and 6 UT in the southern hemisphere and peaks at 14 to 18 UT. In the northern hemisphere the differences in the coverage are less extreme but there is less coverage between 02 and 09 UT and peaks between 11 and 20 UT (Fig. 10d-f). The bias in the DMSP/SSUSI data is not due to seasonal variations in coverage (Fig. 10a-c). The seasonal effect is therefore a feature of the detectability of the TPAs. This means that TPAs have a seasonal dependence on their formation or that there is a seasonal dependence on their visibility such that they are less frequently detected in the summer hemisphere, as will be discussed further below.

The dusk-dawn distribution of the TPAs (Fig. 8a) shows a clear asymmetry with more TPAs being detected at dawn than at dusk. Figure 8b shows dusk-dawn distributions that we have compiled from three other TPA lists (Fear and Milan, 2012a; Hosokawa et al., 2011; Rairden and Mende, 1989); both Hosokawa et al. (2011) and Rairden and Mende (1989) noted the dawn preference in their observations. The comparison between the four studies is interesting as each used different instrumentation to obtain their TPA lists and looked in different hemispheres. Rairden and Mende (1989) and Hosokawa et al. (2011) used ground-based stations but looked at opposite hemispheres. Rairden and Mende (1989) used an image-intensified all-sky camera located at South Pole Station which operated in the optical at 630.0 nm and identified 114 TPA events between April and August 1983-1986. Hosokawa et al. (2011) used an all-sky imager at Resolute Bay, Canada, which operated at 630.0 nm and identified 743 TPAs between January 2005 and December 2009. Fear and Milan (2012a) and this study both used space-based instrumentation. Fear and Milan (2012a) used IMAGE's Far Ultra Violet (FUV) cameras, the wideband imaging camera (WIC) and the Spectrographic Imager 121.8 nm (SI12). IMAGE observed the northern hemisphere aurora between 2000 and 2003, and the southern hemisphere aurora from 2003 to 2005. Between June 2000 and September 2005 and 131 TPAs were identified. Therefore, there does not appear to be a dependence on how the TPA data is collected on the dusk-dawn distributions. From Fig. 8b, it is clear that TPAs are always identified more often

in the dawn sector with approximately a 2:1 ratio. Valladares et al. (1994), who also had TPAs occurring more frequently on the dawn side than the dusk, showed that the convection patterns presented by Potemra et al. (1984) for northward IMF contain a region of convergent electric fields on the dawn side for both positive and negative values of IMF B_Y, suggesting a preponderance of upward current on the dawnside of the polar cap and a region of downward current on the duskside. This might lead to more intense electron fluxes in the dawnside, thus brighter auroral emission and more detectable TPAs.

Linking these findings to the formation models, the closed field line mechanism suggested by Milan et al. (2005) expects the TPAs to be equally viable in both hemispheres as the TPAs in both hemispheres are linked to the same closed field line and the physical structure of the TPA (closed magnetic flux) should be present in both hemispheres. It also expects the TPAs in each hemisphere to be mirrored about the midnight meridian therefore expecting equal numbers of TPAs to form at dusk and at dawn. The findings here then suggest that if the closed field line model is correct a more complicated scenario occurs thus leading to TPAs being detected more often in the dawn sector and in the winter hemisphere. The dusk-dawn distribution in Fig. 8 can still be explained by the convergent electric field on the dawnside and the corresponding upward current creating bright TPAs in the dawn sector.

The preponderance of detected TPAs in the winter hemisphere could be linked to the mapping of closed flux between the two hemispheres. If this mapping is not symmetrical between the two hemispheres both TPAs may not be detectable by the detection algorithm. If the TPA in the winter hemisphere maps to the central polar cap (away from the edge of the auroral oval) while the summer TPA maps closer to the edge of the auroral oval only the winter hemisphere TPA will be detected and appear as a single hemisphere arc. This, though, would raise the question as to why the mapping should occur this way. This could be linked to other factors, such as the IMF B_X component and the dipole tilt of the Earth, but further work would be required to study this.

Alternatively, an interpretation of the fact that some TPAs appear conjugate while others do not is that there are two physical mechanisms at work, and it might be expected that the process of creating a TPA on open field lines is very different from the process of creating a TPA on closed field lines. It could be that these two mechanisms display a seasonal dependence in their occurrence, though we do note that the seasonal distributions of Fig. 7 are not strictly symmetric about the solstices or equinoxes. Another explanation for the annual distributions could be that the TPAs in the summer hemisphere are harder to detect due to a seasonal

dependence on their visibility against the brightness of the sunlit hemisphere. Alternatively, the auroral signature of TPAs may be weaker such that they do not manifest in the summer hemisphere.

We now test whether the occurrence distributions can be interpreted as the likelihood of observing a TPA against a seasonally-dependent background. We assume that the number of TPA events identified in the northern hemisphere and southern hemisphere (Fig. 6) can be interpreted not as a true seasonal variation in the occurrence of TPAs but rather a reflection of probability of seeing TPAs due to visibility and dayglow. Figure 7e shows the number of TPA events seen in the northern hemisphere (red line) and southern hemisphere (blue line) including both conjugate and non-conjugate TPAs (i.e. summed from the distributions in Figs. 7a and b). The purple line is the conjugate only TPAs taken from Fig. 7b. We assume that TPAs occur uniformly throughout the year, and treat the northern and southern distributions as probabilities of seeing an arc if it is present in the given hemisphere. The probabilities are defined such that the probability is one in the month with the greatest number of TPAs detected, therefore the probability is equal to the number of TPAs detected each month divided by the maximum number of TPAs detected in one month. The expected probability of seeing a TPA in both the northern and southern hemisphere conjugately is then the probability of seeing a TPA in the northern hemisphere multiplied by the probability of seeing the TPA in the southern hemisphere (the red and blue lines, multiplied). This is shown by the black dashed line in Fig. 7e, suitably scaled. Fig. 7f is the same analysis but for the UT distributions.

There is fair agreement between the observed conjugate events (purple lines) and the distributions modelled on probabilities (black lines), suggesting that the distribution of the conjugate events can be treated as a visibility issue and as such, there is no need to invoke different formation mechanisms for one-hemisphere and two-hemisphere events. This is supported by the UT distribution (Fig. 7f), which has been shown to be due to a bias in the amount of the detection window scanned by SSUSI. The seasonal variation in visibility could be linked to dayglow contamination of the images, or the conductance of the ionosphere as nightside aurora can be suppressed when the conductance is high for example in the summer hemisphere (Liou et al., 1997; Shue et al., 2001).

On the other hand, if the open field line model is assumed correct there is no need for the TPAs to form simultaneously in both hemispheres or equally at dusk and dawn. If this is the case then the TPAs being detected more often in the dawn can be linked to the upwards currents being preferentially found in the dawn sector. The seasonal dependence could be explained by

the polar cap flow shears, that are linked to the formation of the TPA through the requirement that shears are associated with FACs and hence precipitation, being found preferentially in the winter hemisphere. However, it is unclear why the flow shears would form preferentially in the winter hemisphere.

6 Conclusion

An automated detection algorithm has been developed which allows TPA images to be identified from DMSP/SSUSI data. 5,698 images are identified in the period 2010-2016. A clear seasonal dependence is seen in the TPA images, such that more TPA images are observed in the winter hemisphere. There is also a UT dependence but this is explained by the UT bias in the orbit of the spacecraft. The seasonal dependence is not explained by the orbital bias of the spacecraft. The dusk-dawn distribution shows that TPAs are detected more often in the dawn sector than dusk sector. This distribution is supported by three previous studies, with an approximate 2:1 ratio seen in all four studies. This dawn preference could be linked to the field-aligned current polarity during northward IMF.

Relating the results found here to the open/closed field line arguments, if the Milan et al. (2005) model is correct and all TPAs are associated with closed magnetic flux then we expect the physical structure of TPAs (closed magnetic flux) to be present in both hemispheres simultaneously. Then the possibilities for the seasonal dependence are as follows. The mapping of the closed flux is different in the two hemispheres such that it maps to the middle of the polar cap and appears as a TPA in the winter hemisphere, but is adjacent to the auroral oval in the summer hemisphere, so not clearly a TPA. However, why the winter hemisphere would be preferred is not understood. Another possibility is that more TPAs are seen in the winter because of seasonal changes in their visibility. A final explanation for the seasonal dependence is that the auroral signature of TPAs is seasonally dependent, such they do not as manifest in summer; this could be related to the conductance of the ionosphere.

If instead the open field line model is assumed correct then our observations could be explained if the polar cap flow shears that produce FACs (and hence TPAs) are preferentially found in the winter hemisphere. However, it is unclear why flow shears should form preferentially in the winter hemisphere.

We conclude that further research is needed to determine the exact nature of the seasonal and dawn-dusk dependence of TPAs and to use this information to constrain the formation models.

References

Carlson, H. and Cowley, S. (2005). Accelerated polar rain electrons as the source of sun-aligned arcs in the polar cap during northward interplanetary magnetic field conditions. *Journal of Geophysical Research: Space Physics*, 110(A5).

Carter, J. A., Milan, S. E., Fear, R., Kullen, A., and Hairston, M. (2015). Dayside reconnection under interplanetary magnetic field by-dominated conditions: The formation and movement of bending arcs. *Journal of Geophysical Research: Space Physics*, 120(4):2967–2978.

Carter, J. A., Milan, S. E., Fear, R., Walach, M.-T., Harrison, Z., Paxton, L., and Hubert, B. (2017). Transpolar arcs observed simultaneously in both hemispheres. *Journal of Geophysical Research: Space Physics*, 122(6):6107–6120.

Craven, J., Murphree, J., Frank, L., and Cogger, L. (1991). Simultaneous optical observations of transpolar arcs in the two polar caps. *Geophysical research letters*, 18(12):2297–2300.

Dungey, J. W. (1961). Interplanetary magnetic field and the auroral zones. *Physical Review Letters*, 6(2):47.

Fear, R. and Milan, S. (2012a). The IMF dependence of the local time of transpolar arcs: Implications for formation mechanism. *Journal of Geophysical Research: Space Physics*, 117(A3).

Fear, R. and Milan, S. (2012b). Ionospheric flows relating to transpolar arc formation. *Journal of Geophysical Research: Space Physics*, 117(A9).

Hardy, D., Burke, W., and Gussenhoven, M. (1982). Dmsp optical and electron measurements in the vicinity of polar cap arcs. *Journal of Geophysical Research: Space Physics*, 87(A4):2413–2430.

Hosokawa, K., Kullen, A., Milan, S., Reidy, J., Zou, Y., Frey, H. U., Maggiolo, R., and Fear, R. (2020). Aurora in the polar cap: A review. *Space Science Reviews*, 216(1):1–44.

Hosokawa, K., Moen, J., Shiokawa, K., and Otsuka, Y. (2011). Motion of polar cap arcs. *Journal of Geophysical Research: Space Physics*, 116(A1).

Huang, C., Craven, J., and Frank, L. (1989). Simultaneous observations of a theta aurora and associated magnetotail plasmas. *Journal of Geophysical Research: Space Physics*, 94(A8):10137–10143.

King, J. and Papitashvili, N. (2005). Solar wind spatial scales in and comparisons of hourly wind

and ace plasma and magnetic field data. *Journal of Geophysical Research: Space Physics*, 110(A2).

Kullen, A., Brittnacher, M., Cumnock, J., and Blomberg, L. G. (2002). Solar wind dependence of the occurrence and motion of polar auroral arcs: A statistical study. *Journal of Geophysical Research: Space Physics*, 107(A11):13–1.

Kullen, A., Fear, R., Milan, S. E., Carter, J., and Karlsson, T. (2015). The statistical difference between bending arcs and regular polar arcs. *Journal of Geophysical Research: Space Physics*, 120(12):10–443.

Liou, K., Newell, P., Meng, C.-I., Brittnacher, M., and Parks, G. (1997). Synoptic auroral distribution: A survey using polar ultraviolet imagery. *Journal of Geophysical Research: Space Physics*, 102(A12):27197–27205.

Milan, S. E., Hubert, B., and Grocott, A. (2005). Formation and motion of a transpolar arc in response to dayside and nightside reconnection. *Journal of Geophysical Research: Space Physics*, 110(A1).

Obara, T., Kitayama, M., Mukai, T., Kaya, N., Murphree, J., and Cogger, L. (1988). Simultaneous observations of sun-aligned polar cap arcs in both hemispheres by exos-c and viking. *Geophysical Research Letters*, 15(7):713–716.

Østgaard, N., Mende, S., Frey, H., Frank, L., and Sigwarth, J. (2003). Observations of non-conjugate theta aurora.

Paxton, L. J., Meng, C.-I., Fountain, G. H., Ogorzalek, B. S., Darlington, E. H., Gary, S. A., Goldsten, J. O., Kusnierkiewicz, D. Y., Lee, S. C., Linstrom, L. A., et al. (1992). Special sensor ultraviolet spectrographic imager: An instrument description. In *Instrumentation for planetary and terrestrial atmospheric remote sensing*, volume 1745, pages 2–15. International Society for Optics and Photonics.

Paxton, L. J., Meng, C.-I., Fountain, G. H., Ogorzalek, B. S., Darlington, E. H., Gary, S. A., Goldsten, J. O., Kusnierkiewicz, D. Y., Lee, S. C., Linstrom, L. A., et al. (1993). Ssusi: Horizon-to-horizon and limb-viewing spectrographic imager for remote sensing of environmental parameters. In *Ultraviolet technology IV*, volume 1764, pages 161–176. International Society for Optics and Photonics.

Paxton, L. J., Schaefer, R. K., Zhang, Y., and Kil, H. (2017). Far ultraviolet instrument technology. *Journal of Geophysical Research: Space Physics*, 122(2):2706–2733.

Potemra, T., Zanetti, L., Bythrow, P., Lui, A., and Iijima, T. (1984). By-dependent convection patterns during northward interplanetary magnetic field. *Journal of Geophysical Research: Space Physics*, 89(A11):9753–9760.

Rairden, R. and Mende, S. (1989). Properties of 6300-å auroral emissions at south pole. *Journal of Geophysical Research: Space Physics*, 94(A2):1402–1416.

Reidy, J. A., Fear, R., Whiter, D., Lanchester, B., Kavanagh, A. J., Milan, S., Carter, J., Paxton, L., and Zhang, Y. (2018). Interhemispheric survey of polar cap aurora. *Journal of Geophysical Research: Space Physics*, 123(9):7283–7306.

Shi, Q., Zong, Q.-G., Fu, S., Dunlop, M., Pu, Z., Parks, G., Wei, Y., Li, W., Zhang, H., Nowada, M., et al. (2013). Solar wind entry into the high-latitude terrestrial magnetosphere during geomagnetically quiet times. *Nature communications*, 4(1):1–6.

Shinohara, I. and Kokubun, S. (1996). Statistical properties of particle precipitation in the polar cap during intervals of northward interplanetary magnetic field. *Journal of Geophysical Research: Space Physics*, 101(A1):69–82.

Shue, J.-H., Newell, P., Liou, K., and Meng, C.-I. (2001). The quantitative relationship between auroral brightness and solar euv pedersen conductance. *Journal of Geophysical Research: Space Physics*, 106(A4):5883–5894.

Valladares, C., Carlson Jr, H., and Fukui, K. (1994). Interplanetary magnetic field dependency of stable sun-aligned polar cap arcs. *Journal of Geophysical Research: Space Physics*, 99(A4):6247–6272.

Xing, Z., Zhang, Q., Han, D., Zhang, Y., Sato, N., Zhang, S., Hu, Z., Wang, Y., and Ma, Y. (2018). Conjugate observations of the evolution of polar cap arcs in both hemispheres. *Journal of Geophysical Research: Space Physics*, 123(3):1794–1805.

Zhang, Y., Paxton, L., Zhang, Q., and Xing, Z. (2016). Polar cap arcs: Sun-aligned or cusp-aligned? *Journal of Atmospheric and Solar-Terrestrial Physics*, 146:123–128.

Zhu, L., Schunk, R., and Sojka, J. J. (1997). Polar cap arcs: A review. *Journal of Atmospheric and Solar-Terrestrial Physics*, 59(10):1087–1126.

Acknowledgements

GEB is supported by a Science and Technology Facilities Council (STFC), UK, studentship. SEM is supported by STFC grant no. ST/S000429/1. The work at the Birkeland Centre for Space Science is supported by the Research Council of Norway under contract 223252/F50. We

634 acknowledge use of NASA/GSFC's Space Physics Data Facility's CDAWeb service and OMNI
635 data (at http://cdaweb.gsfc.nasa.gov). The DMSP/SSUSI file type EDR-AUR data were ob-
636 tained from http://ssusi.jhuapl.edu (data version 0106, software version 7.0.0, calibration period
637 version E0018).